Implementation of 3-Port Condensing Wave Rotors in R718 Cycles

Amir A. Kharazi
e-mail: amir.kharazia@jacobs.com

Pezhman Akbari
e-mail: akbari@egr.msu.edu

Norbert Müller
e-mail: mueller@egr.msu.edu

Department of Mechanical Engineering,
Michigan State University,
Engineering Building,
East Lansing, Michigan 48824-1226

The use of a novel 3-port condensing wave rotor is suggested to enhance the turbocompression in a refrigeration cycle that works only with water (R718) as a refrigerant. Although the implementation of such a wave rotor essentially reduces the size and cost of R718 units, their efficiency may also be increased. The condensing wave rotor employs pressurized water to pressurize, desuperheat, and condense the refrigerant vapor, all in one dynamic process. The underlying phenomena of flash evaporation, shock wave compression, desuperheating, and condensation inside the wave rotor channels are described in a wave and phase-change diagram. The thermodynamic process is shown in pressure-enthalpy and temperature-entropy diagrams. Based on the described thermodynamic model, a computer program was generated to evaluate the performance of R718 baseline and wave-rotor-enhanced cycles. The effect of some key parameters on the performance enhancement is demonstrated as an aid for optimization. A performance map summarizes the findings. It shows optimum wave rotor pressure ratio and maximum relative performance improvement of R718 cycles by using the 3-port condensing wave rotor.
[DOI: 10.1115/1.2131886]

Keywords: 3-port condensing wave rotor, water as a refrigerant, R718, refrigeration, shock wave, flash evaporation, wave rotor technology

Introduction

There has been a tremendous effort by the refrigeration and air-conditioning industry to find the best substitute for chlorofluorocarbon (CFC) refrigerants [1,2]. The search for new and environmentally benign refrigerants has renewed interest in technologies that use natural refrigerants, such as water (R718). Considering all pros and cons of natural refrigerants already described in previous studies [3,4], water can be considered as an attractive refrigerant because of its following advantages:

- It has no global warming potential (GWP=0).
- It has no ozone depletion potential (ODP=0).
- It is nontoxic, nonflammable, easy to handle, and inert to the environment (minimizes safety precautions).
- It has no risk of future restrictions due to refrigerant environmental impact.
- It has no disposal problem after use.
- It works with very low pressure differences, reducing safety precautions.
- It has high theoretical coefficient of performance (COP), competitive with CFCs depending on the evaporatoration temperature [5,6].
- The system working with water as a refrigerant can use direct heat exchangers for evaporation and condensation. Therefore, R718 systems can obtain very high COP [7].
- Tap water, treated waste water, or coarsely filtered river water can be used directly as make-up water (warehousing bulky refrigeration canisters is not required).
- Chiller systems, coupled with a closed cooling tower loop, allow for diminished water treatment.
- Turbochillers using water as a refrigerant have shown to be inherently much less noisy than conventional compression chiller systems.

Despite the above attractive features, there are a few challenges of using water as a refrigerant compared to traditional refrigerants. At the triple point, the vapor pressure of water is only 611 Pa, which is <1% of the atmospheric pressure. The low operating pressures of water-vapor refrigeration systems combined with the steep vapor pressure curve of water requires compression systems that can handle large-volume flows while still delivering high-pressure ratios [8–11]. This states challenges for the compressor design. Although single-stage turbo compressors commonly deliver large-volume flows with mostly insufficient pressure ratios, positive displacement compressors can obtain high-pressure ratios but only for relative small-volume flows. A technical compromise has been the use of multistage turbocompressors with intercooler [12].

Water Refrigeration Cycles. Figure 1 pictures the schematic of a two-stage R718 turbochiller with direct condensation and evaporation, two high-performance centrifugal compressors, and an intercooler. Figure 2 is a schematic thermodynamic model for the actual system. R718 units can be comprised of three directly interlinked cycles: (i) a cooling water cycle that condenses the superheated vapor from the compressor and releases the thermal energy to the ambient through a heat exchanger device, mostly a cooling tower; (ii) a chilled water cycle that absorbs thermal energy from the heat source and transfers it to the refrigerant by phase change; and (iii) a refrigerant cycle or the core cycle that consists of four components: compressor, expansion device, condenser, and evaporator. Cooling towers can be direct (open-circuit) or indirect (closed-circuit) heat rejection equipment. In the direct type, cooling water is exposed directly to the atmosphere. The warm cooling water is sprayed over a fill that increases the contact area, and air is blown through the fill. The majority of heat removed from the cooling water is due to partial evaporation of the cooling water requiring a permanent replenishment. The re-

Contributed by the Advanced Energy Systems Division of ASME for publication in the JOURNAL OF ENERGY RESOURCES TECHNOLOGY. Manuscript received April 2, 2004; final manuscript received September 28, 2005. Review conducted by Srinivas Garimella.

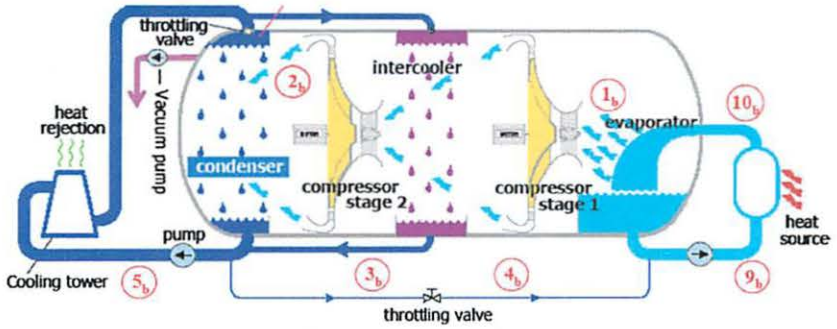

Fig. 1 Schematic of a R718 chiller unit with direct condensation and evaporation

maining cooled water drops into a collection basin and is recirculated to the chiller. Using such an open circuit, a pump is required before the cooling tower to pump the water out of condenser at subambient pressure to somewhat above ambient pressure. In this case, considerable throttling occurs after the cooling tower when the water enters the condenser under vacuum, which is shown by a throttling valve in Fig. 1. The use of direct heat exchangers may result in contamination of the refrigerant with noncondensable gases, solids, or entrained liquids [10]; therefore, using indirect heat exchangers may reduce the cost associated with degasifiers and cleaning. There are two options for realization, which can be used alternatively or combined. First, an indirect cooling tower can be employed in which water circulates through tubes (coils) located in the tower without coming in contact with the outside air and pressure. The cooling-tower heat transfer still may be enhanced as needed by wetting the outside of the coils utilizing evaporative cooling. If an indirect cooling tower (closed circuit) is used, the pump needs only to overcome the pressure loss in the cooling circuit and throttling losses at the entrance to the evaporator can be minimized. In such a case, the pump can be placed before or after the cooling tower, depending on where pump cavitation is prevented best considering the competing effects of temperature drop and pressure loss across the cooling tower. Second, the cooling tower can be separated from the chiller unit using effective plate heat exchangers. These typically introduce only 1 K additional temperature difference, which adds to the ~1 K temperature difference in the internal direct heat exchanger (condenser). This is still superior to an internal indirect condensing heat exchanger, which may typically introduce a temperature difference of ~5 K.

Disadvantages of the current state-of-the-art R718 units (Fig. 1) are mainly their size and cost. The size is due to the use of two centrifugal compressors with comparably large diameters and voluminous (same diameter) internal direct heat exchangers. The cost is mainly generated by the two relative expensive compressors with independent variable speed drives. An additional challenge has been obtaining high peak compressor pressure ratios for high temperature lift. One reason has been the limited compressor efficiency that results from the special wheel construction and the limited pressure recovery of the steady-state diffuser, which decelerates the high-speed vapor flow out of the high-performance wheel. Low Reynolds numbers of water vapor under vacuum (300 times lower than if R134a or R12 are used) [11] are an additional challenge for achieving a high efficiency. The presented work is part of the ongoing research to improve the compressors and heat exchangers and to reduce the size and cost of the whole unit.

R-718 Refrigeration Cycle Enhanced With a 3-Port Condensing Wave Rotor

The potential for using wave devices in thermodynamic cycles for power generation, propulsion, and refrigeration has attracted the attention of researchers since the early twentieth century. Shock tubes, shock tunnels, pressure exchangers, pulse combustors, pulse detonation engines, and wave rotors are among the best-known wave devices developed thus far. These devices represent applications of classical nonsteady, one-dimensional compressible flow theory. It is well known, but not yet widely employed, that time-dependent flow devices can generate much greater pressure rises than those obtained in steady-state flow devices [13–15]. By generating shock waves in appropriate geometries, unsteady wave machines can transfer the energy of a high-pressure fluid directly to another low-pressure fluid without using mechanical components, such as pistons or vaned impellers.

Within the family of wave devices, wave rotors have demonstrated a favorable potential for reaching the ultrahigh perfor-

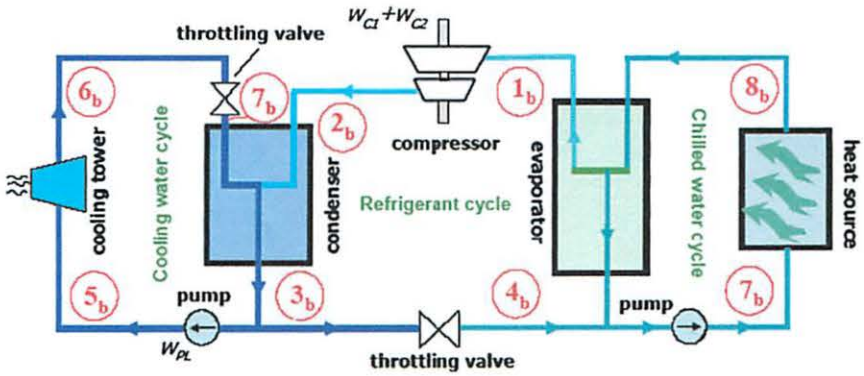

Fig. 2 Schematic of thermodynamic model of a R718 chiller unit with a two-stage compressor and a direct condenser

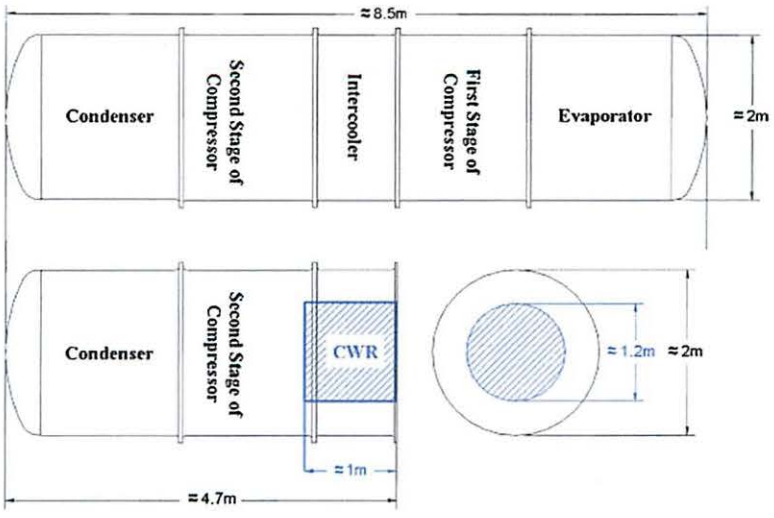

Fig. 3 Size reduction by combining intercooler, second-stage compression, and condensation into a condensing wave rotor (CWR)

mance targets of power systems and for lowering their cost. Much research has been devoted to the progress and development of wave rotor technology, especially in the past few decades. Most of the work in the U.S. expands from the early efforts of the General Electric Company (GE), General Power Corporation (GPC), and Rolls Royce [16,17] to the recent activities of the wave rotor team at NASA Glenn Research Center (GRC), collaborated by the U.S. Army Research Laboratory (ARL) and Rolls-Royce Allison [18–27].

The present study demonstrates the enhancement of a turbocompression refrigeration cycle that uses water as refrigerant (R718) by utilizing a novel 3-port condensing wave rotor. Adding a wave rotor to a R718 cycle enables greater temperature lift or reduces the compressor pressure ratio, which is crucial for the R718 chiller technology, where the stage pressure ratio is very much limited by the thermodynamic properties of water vapor. Some structural and economic advantages of integrating both 4-port and 3-port wave rotors in a R718 cycle have been discussed in a previous study [15]. Using a 3-port condensing wave rotor in a water refrigeration cycle can improve the coefficient of performance of R718 units [28] while reducing their size and cost. Its successful implementation may replace three subsystems: the intercooler, one compressor stage, and the condenser. With conservative measures as shown in Fig. 3, this may reduce the overall size of the R718 unit to nearly 50%, since the volume of these three subsystems reduces down to about one-tenth of the current size [29]. It is noted that the wave rotor length is a design parameter that adjusts with rotational speed and the speed of sound within the fluid. The wave rotor diameter is governed by the volume flow rate of the precompressed vapor out of first compressor stage into the condensing wave rotor and the number of wave cycles per revolution. A schematic thermodynamic model of a R718 cycle using a 3-port condensing wave rotor is depicted in Fig. 4. In this innovative design, condensation of vapor occurs inside the wave rotor channels as explained below.

Although Fig. 5 shows a schematic of a 3-port condensing wave rotor, Fig. 6 schematically shows the regions modeled for a channel during compression and condensation. The following explanation follows the points (states) introduced in Fig. 4. Coming from the turbocompressor (2), the superheated vapor flows continuously through a vapor collector (shown in Fig. 5) to the inlet port of the wave rotor located at one of the two stationary end plates. By rotating the wave rotor between the two end plates, the wave rotor channels are opened to the port and filled with the incoming superheated vapor. Region (*a*) in Fig. 6 is the state after

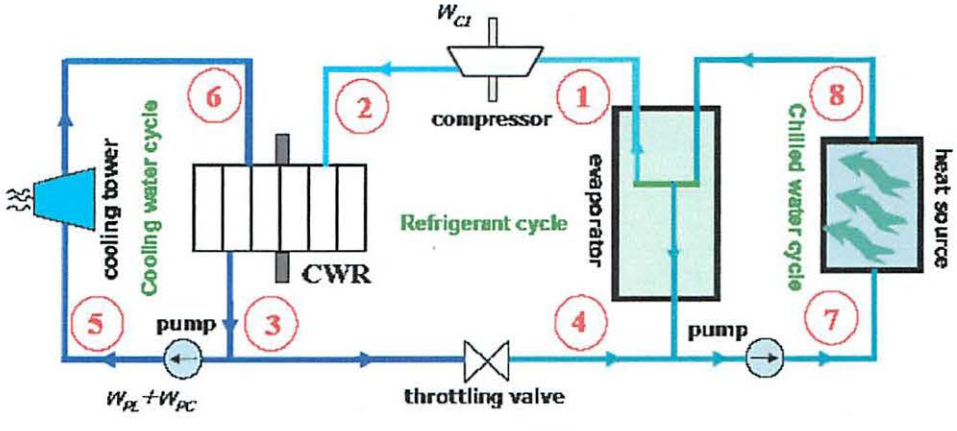

Fig. 4 Schematic of the thermodynamic model of a R718 chiller unit enhanced by a 3-port condensing wave rotor (CWR) substituting for the condenser and for one stage of compressor

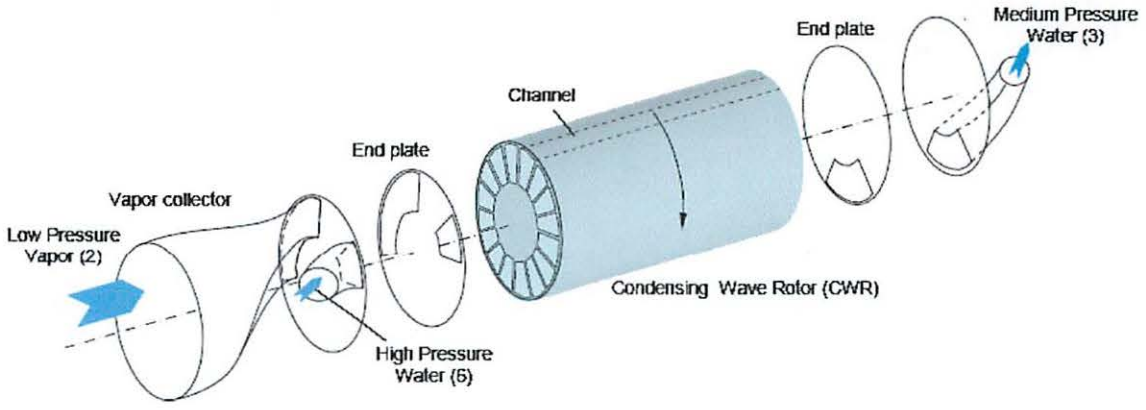

Fig. 5 Schematic of a 3-port condensing wave rotor

the filling process is completed. After further rotation, the channels meet the second-inlet port (6) through which the high-pressure low-temperature water (*e*) comes in and is exposed to the low-pressure high-temperature superheated vapor in region (*a*). Because of the sudden pressure drop (from p_6 to p_2), all the heat cannot be contained in the incoming water as sensible heat, and the heat surplus is transformed into latent heat of vaporization. This is the so-called flash evaporation or flashing phenomenon [30,31]. Therefore, one portion of the incoming water suddenly vaporizes (*c*) and the remaining part cools down (*d*). The frontal area of the saturated vapor (*c*) generated by the flash evaporation is called the contact interface and acts like a fast-moving piston. It causes a shock wave triggered from the leading edge of the inlet port traveling through the superheated low-pressure vapor, which exists inside the channel (*a*). The shock wave travels with supersonic speed (V_{shock}) faster than the contact interface ($V_{interface}$). Therefore, the trajectory of the shock wave (solid line in Fig. 6) has a smaller slope than the incoming water and the contact interface of the generated vapor (dashed line). Behind the moving shock wave (*b*), the temperature is increased from T_2 to $T_{2'}$ and the pressure is increased from p_2 to $p_{2'}=p_3$ due to the shock compression. The latter is a design decision similar to a tuning condition. With it, the pressure at the inlet port p_6 is set to an appropriate value that generates the pressure ratio p_6/p_2 required to trigger the desired shock wave. The superheated vapor will be

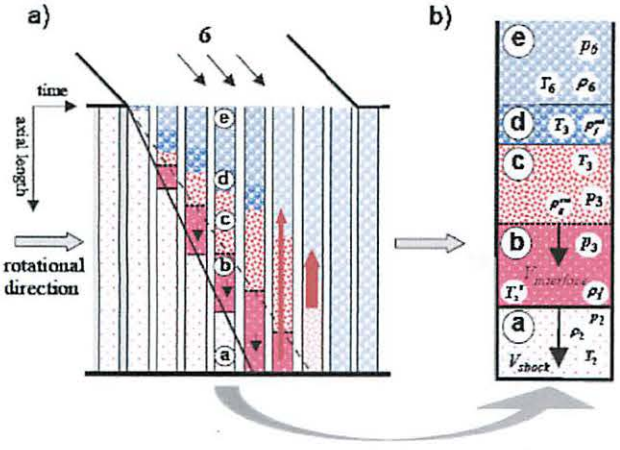

Fig. 6 (*a*) Schematic wave and phase-change diagram for the 3-port condensing wave rotor (high pressure part) and (*b*) A magnified channel showing the regions modeled during compression and condensation

condensed at pressure p_3. This shows that the fluid in its liquid state serves as a "work capacitor" storing pump work to release it during its expansion in the wave rotor channels for the simultaneous vapor compression. Therefore, in the enhanced system the pump in the cooling water cycle not only has to provide the work necessary to overcome the pressure loss in the heat rejecter cycle w_{PL}, but also the work necessary for the shock wave compression in the wave rotor channels w_{PC}. The pressure behind the shock wave (*b*) is imposed on the vapor generated by the flash evaporation (*c*). It is the pressure at the water surface and the equilibrium pressure at which the evaporation decays $p(c)=p(b)=p_3$. Hence, both generated vapor and the cooled water obtain the saturation temperature $T_3=T_{sat}(p_3)$.

Because of the direct contact of the superheated compressed vapor (*b*) with the cold incoming water (*e*), the superheated vapor is desuperheated and its heat is transferred (*f*) to the incoming water. This continues until the equilibrium temperature T_3 is achieved in region (*b*) and the superheated vapor is changed to saturated vapor. Subsequently, the incoming water compresses the saturated vapor further and condenses it, while the latent heat is transferred to the incoming water (*g*). The water, which is nearly a fully condensed two-phase vapor with a typical quality of 0.005, is scavenged through the only outlet of the wave rotor (3). The scavenging process may be supported by gravity and pump power.

The schematic pressure-enthalpy (*p-h*) and temperature-entropy (*T-s*) diagrams of both the baseline and the wave-rotor-enhanced cycle are depicted in Figs. 7 and 8, respectively. Both cycles start at the outlet of the evaporator (state 1), where the vapor is saturated. State 2_b represents the compressor outlet of the baseline cycle, whereas state 2 is the compressor outlet of the wave-rotor-enhanced cycle, which allows using a compressor with a lower pressure ratio. State 2′ is an intermediate state inside the wave rotor channels that corresponds to the flow properties in region (*b*) right after the shock wave. The slope between states 2 and 2′ is greater than that between states 1 and 2_b because the shock compression typically occurs with a higher efficiency [13–15]. Still inside the wave rotor channel, the superheated vapor is desuperheated to the equilibrium temperature T_3 ($2' \rightarrow 3$). State 3 is actually much closer to the liquid region than shown in Figs. 7 and 8 because the mass flow rate of the cooling water cycle ($\dot{m}_6$) is much greater than that of the core cycle ($\dot{m}_2$). Knowing this, it becomes clear why the distances between states 3, 5, and 6 are magnified in this schematic diagram. The expansion process ($6 \rightarrow 3$) releases the energy consumed by the compression process of the vapor ($2 \rightarrow 2'$) all within the wave rotor channels. Coming from the only outlet port of the wave rotor (state 3), the flow diverges. The small fraction used as refrigerant is directed to the

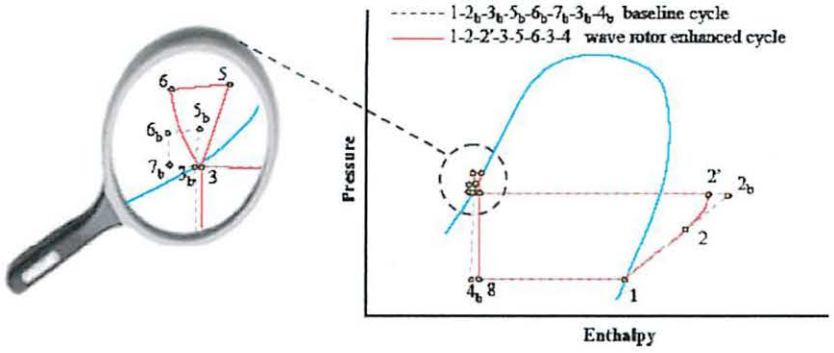

Fig. 7 Schematic *p-h* diagram of a R718 baseline cycle and enhanced cycle with a 3-port condensing wave rotor

expansion valve and is expanded in a constant enthalpy process ($3 \rightarrow 4$), while largest part of the flow out of the wave rotor is pumped ($3 \rightarrow 5$), providing the energy for the vapor compression in the wave rotor w_{PC} and compensating for the pressure loss in the heat rejecter and associated piping w_{PL}. In this case, an inducer pump may be used to avoid cavitations problems. Then, the fluid goes into the heat rejecter (cooling tower or similar) where it cools off ($5 \rightarrow 6$). In the enhanced cycle, the inlet port of condensing wave rotor can be viewed as throttling; therefore, a separate expansion valve is not shown. In difference to the insenthalpic expansion (throttling), in the condensing wave rotor most of the pressure is recovered immediately for compression of the refrigerant gas in the channels of a condensing wave rotor. The expansion in the condensing wave rotor can be viewed as a turbine expansion in which the work necessary for refrigerant compression is extracted.

Figure 9 pictures one possible integration of a condensing wave rotor in a R718 cycle. This innovative design unifies a significant part of the compression with the desuperheating and condensation of the refrigerant vapor in a compact dynamic unit. Such innovative designs of R718 chillers with integration of condensing wave rotors will result in manufacturable, easily scalable (3–300 kW), and high-efficient refrigeration cycles.

Performance Evaluation

A computer code based on the thermodynamic model described below is generated for performance evaluation of R718 refrigeration cycles enhanced with 3-port condensing wave rotors. The evaporator temperature T_1 and heat rejecter temperature T_3 are commonly fixed by the application. The objective is to get the highest increase in coefficient of performance (COP_{gain}) compared to the baseline cycle. Independent design parameters are the mass flow ratio ($K=\dot{m}_6/\dot{m}_2$), which relates the mass flow of the cooling cycle to the mass flow of the core cycle, and the pressure ratio of the wave rotor ($PR_W=p_3/p_2$).

Additional assumptions considered in the thermodynamic model are as follows:

- For comparison of baseline and enhanced cycles, the evaporator and condenser inlet temperatures are considered the same ($T_1=T_{1b}$ and $T_3=T_{3b}$).
- Temperature difference across the heat rejecter is kept constant ($T_6-T_5=3$ K).
- Pressure drop in heat exchanger, evaporator, and pipes is neglected.
- Condenser and evaporator outlet states are fully saturated.
- The same polytropic compressor efficiency is used for baseline and enhanced cycles. Its value of 0.72 is obtained by assuming an isentropic efficiency of 0.7 for a compressor with a pressure ratio of 2.
- The superheated vapor is considered as an ideal gas ($\gamma = 1.33$).
- One-dimensional gas-dynamic shock wave equations are used to calculate the flow properties across the moving normal shock wave. Reflected shock waves are not considered.
- The hydraulic efficiency of the pump is 0.9.
- Liquid water is considered as incompressible.

The Baseline Cycle. In the ideal vapor-compression refrigeration cycle shown in Fig. 2, refrigerant from the evaporator flows into the compressor as a saturated vapor, then it discharges into the condenser as a superheated vapor. The saturated liquid refrigerant at the condenser outlet returns to the evaporator through the expansion valve and then cycle repeats.

As shown in Table 1, saturation temperatures at the evaporator

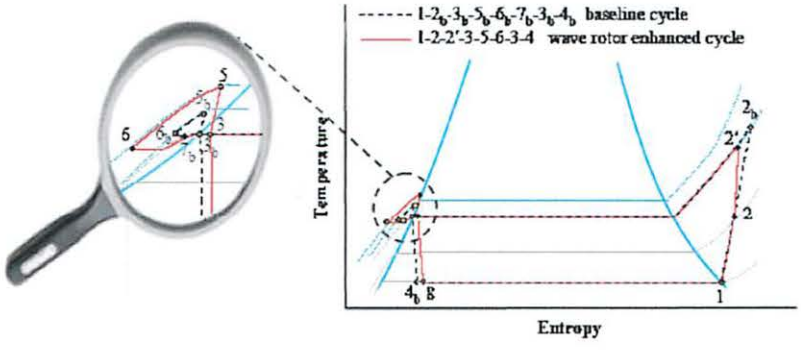

Fig. 8 Schematic *T-s* diagram of a R718 baseline cycle and enhanced cycle with a 3-port condensing wave rotor

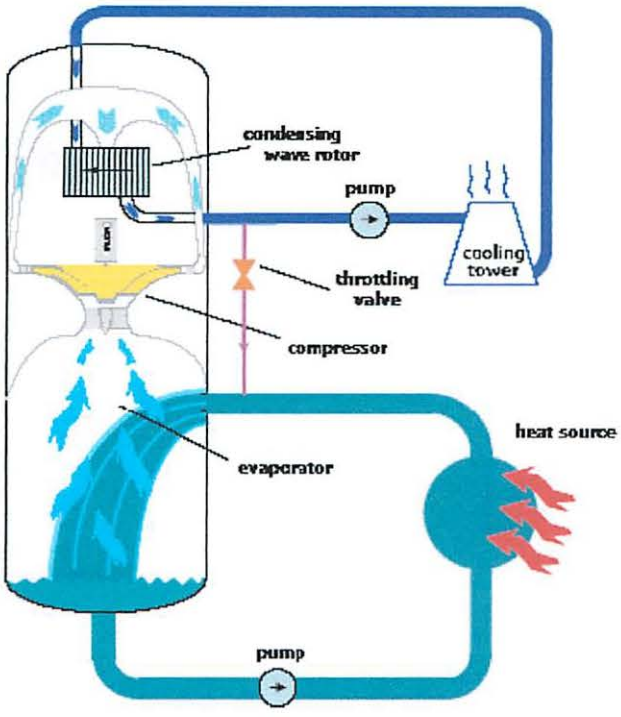

Fig. 9 Novel compact R718 water chiller with integration of a condensing wave rotor

and the condenser are the input data for this analysis. To obtain the COP of the cycle, the thermodynamic states at each location are determined sequentially as follows:

Compressor Inlet (State 1).

$$T_1 = T_e$$
$$p_1 = p_{\text{sat}}(T_e) \tag{1}$$
$$h_1 = h_{\text{sat},v}(T_e)$$

Condenser Outlet (State 3_b).

$$T_{3b} = T_c$$
$$p_{3b} = p_{\text{sat}}(T_c) \tag{2}$$
$$h_{3b} = h_{\text{sat}}(T_c)$$

Compressor Outlet (State 2_b). The cycle overall pressure ratio is calculated by

$$\Pi_b = \frac{p_{3b}}{p_1} \tag{3}$$

and the enthalpy change across the compressor, assuming an average specific heat, is obtained by

Table 1 Input data for the baseline cycle analysis

Input data for the baseline cycle	
Saturation temperature of the evaporator	T_e
Saturation temperature of the condenser	T_c

Table 2 Input data for the enhanced cycle analysis

Input data for enhanced cycle	
Saturation temperature of the evaporator	T_e
Saturation temperature of the condenser	T_c
Temperature drop in the condenser	ΔT_c
Mass flow ratio between chilled water cycle and the cooling water cycle	K
Pressure ratio of the baseline cycle	Π_b
Pressure ratio of the wave rotor	PR_W
Hydraulic efficiency of the pump	η_p

$$\Delta h = \left(\frac{1}{\eta_C}\right) C_p T_1 [(\Pi_b)^{(\gamma-1)/\gamma} - 1] \tag{4}$$

where compressor isentropic efficiency η_C is calculated by assuming a polytropic efficiency of 0.7. Therefore, thermodynamic properties of the compressor outlet are

$$h_{2b} = h_1 + \Delta h$$
$$p_{2b} = p_{3b} \tag{5}$$
$$T_{2b} = T(p_{2b}, h_{2b})$$

Expansion Valve Outlet (State 4_b).

$$h_{4b} = h_{3b}$$
$$p_{4b} = p_1 \tag{6}$$
$$T_{4b} = T(p_{4b}, h_{2b})$$

By definition COP is the ratio between the processed heat at the evaporator ($q_L = h_1 / h_{4b}$) to the work consumed by the compressor ($w_c = h_{2b} - h_1$)

$$\text{COP} = \frac{q_L}{w_c} \tag{7}$$

The Enhanced Cycle. As shown in Fig. 4 in the enhanced cycle, the superheated vapor leaving the compressor discharges into the wave rotor. The pressure ratio of the compressor is less than that of the baseline engine. After the compression of the superheated vapor in the wave rotor, one portion of the almost saturated water at the wave rotor exit (3) goes to the heat exchanger, whereas the other portion returns to the evaporator through the expansion valve.

The input data for analysis of the enhanced cycle are given in Table 2. To obtain the COP of the enhanced cycle, the thermodynamic states at each location can be obtained sequentially as follows:

Compressor Inlet (State 1). The compressor inlet condition at state 1 is the same as the baseline cycle.

Wave Rotor Outlet (State 3). The wave rotor outlet flow is in the saturation region, very close to the saturated liquid line. Therefore,

$$T_3 = T_c$$
$$p_3 = p_{\text{sat}}(T_c) \tag{8}$$

Considering a control volume around the wave rotor, the conservation of mass law gives

$$\dot{m}_2 + \dot{m}_6 = \dot{m}_3 \tag{9}$$

and conservation of energy implies

$$h_2\dot{m}_2 + h_6\dot{m}_6 = h_3\dot{m}_3 \tag{10}$$

Using the definition of mass flow ratio ($K=\dot{m}_6/\dot{m}_2$), Eqs. (9) and (10) can be combined as

$$h_3 = \left(\frac{1}{1+K}\right)(h_2 + h_6 K) \tag{11}$$

The enthalpy at state 6 will be calculated later.

Evaporator Inlet (State 4).

$$p_4 = p_1$$

$$h_4 = h_3 \tag{12}$$

$$T_4 = T(p_4 h_4)$$

and the quality of liquid is calculated by

$$x_4 = \frac{h_4 - h_{\text{sat}}(T_e)}{h_{\text{sat}}(T_e) - h_{\text{sat}}(T_c)} \tag{13}$$

Compressor Outlet (State 2). The compressor exit pressure is calculated by

$$p_2 = \frac{\Pi_b}{PR_W} \tag{14}$$

and Eq. (4) is used to calculate the enthalpy at the compressor exit, substituting the new value of compressor exit pressure. Therefore,

$$h_2 = h_1 + \Delta h$$

$$T_2 = T(p_2, h_2) \tag{15}$$

Shock Wave Compression (State 2'). As described above, due to the sudden pressure drop from p_6 to p_2, flash evaporation generates a shock wave triggered from the leading edge of the inlet port traveling through the superheated low-pressure vapor, which exists inside the channel. Therefore, the temperature is increased from T_2 to $T_{2'}$ and the pressure is increased from p_2 to $p_{2'}=p_3$. Using moving normal shock relations, temperature increase is calculated by [32]

$$T_{2'} = T_2 \frac{p_3}{p_2}\left[\frac{\frac{p_3}{p_2} + \frac{\gamma+1}{\gamma-1}}{1 + \frac{\gamma+1}{\gamma-1}\frac{p_3}{p_2}}\right] \tag{16}$$

and

$$p_{2'} = p_3$$

$$h_{2'} = h(T_{2'}, p_{2'}) \tag{17}$$

Pump Outlet (State 5). As stated above, the pressure (p_5) provided by the pump in the cooling water cycle is used to generate the pressure ratio p_6/p_2 required to trigger the desired shock wave. Therefore,

$$\Delta p = (h_{2'} - h_2)\frac{\rho_5}{K} \tag{18}$$

where liquid water is considered incompressible; therefore, $\rho_5 = p_3 = \rho(T_3, p_3)$. Thus,

$$p_5 = p_3 + \Delta p \tag{19}$$

and the enthalpy increase by the pump is

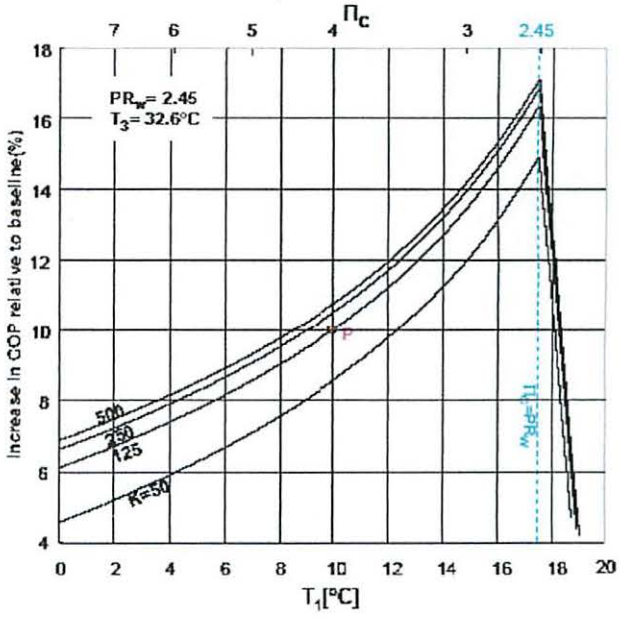

Fig. 10 Relative COP increase versus evaporation temperature for different mass flow ratios

$$\Delta h = \frac{\Delta p}{\rho_5 \eta_h} \tag{20}$$

where η_h is hydraulic efficiency of the pump. Therefore,

$$h_5 = h_3 + \Delta h$$

$$T_5 = T(p_5 h_5) \tag{21}$$

Heat Exchanger (Cooling Tower) Outlet (State 6). For the indirect cooling tower, the temperature drop across the cooling tower is assumed ΔT_c (see Table 2); therefore,

$$T_6 = T_5 - \Delta T_c$$

$$p_6 = p_5 \tag{22}$$

$$h_6 = h(T_6, p_6)$$

Finally, COP for the enhanced cycle is obtained by

$$\text{COP} = \frac{q_L}{w_c + w_p K} \tag{23}$$

where

$$q_L = h_1 - h_4$$

$$w_c = h_2 - h_1 \tag{24}$$

$$w_p = h_5 - h_3$$

Results and Discussions

Figure 10 shows the percentage increase in COP relative to baseline versus the evaporator temperature (T_1) for different mass flow ratios K. By increasing evaporator temperature T_1, the COP of the wave-rotor-enhanced cycle is increased relative to the COP of the baseline cycle. This trend is seen until the compressor pressure ratio in the enhanced cycle ($\Pi_c = p_2/p_1$) is reduced to a value that is equal to the wave rotor pressure ratio ($\Pi_c = PR_W$). After that, the relative COP_{gain} drops dramatically.

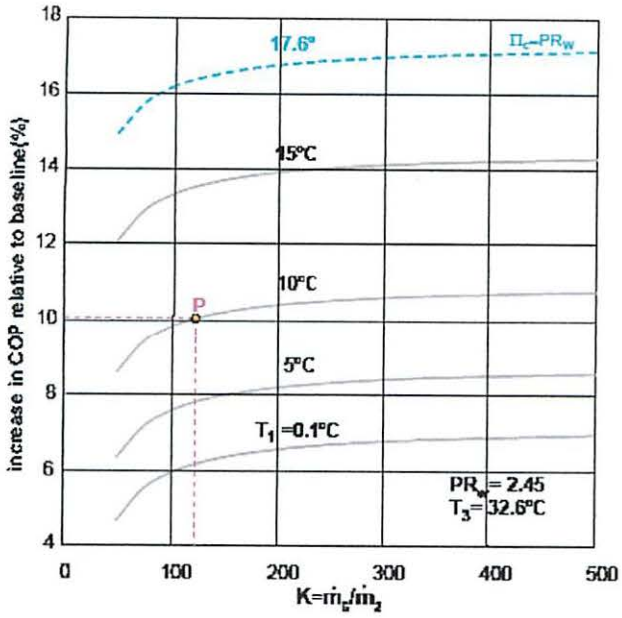

Fig. 11 Relative COP increase versus mass flow ratio for different evaporation temperatures

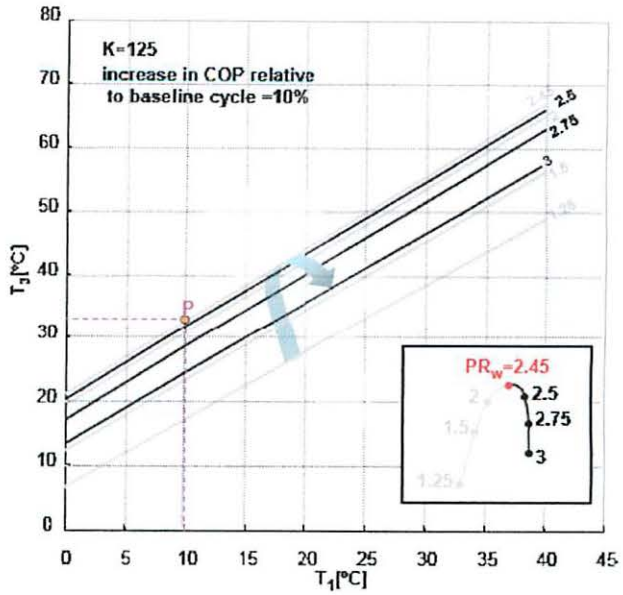

Fig. 13 Heat rejecter temperature versus evaporator temperature for different wave rotor pressure ratios

Figure 11 represents the percentage increase in COP relative to baseline versus mass flow ratio K for different evaporator temperatures, such as a side view of Fig. 10. It shows only the increasing branches of Fig. 10 up to an evaporation temperature where the pressure ratio of the turbo compressor is reduced to the value of the wave rotor pressure ratio. Increasing the mass flow ratio above 200 appears as ineffective according to Fig. 11.

Figure 12 shows the effect of the wave rotor pressure ratio (PR_W) on the percentage increase in COP relative to baseline for different mass flow ratios K. Each curve has a maximum point that indicates the best choice of wave rotor pressure ratio for the given system specifications. The location of this point depends on several parameters, including the hydraulic efficiency of the pump, compressor polytropic efficiency, evaporator temperature, and temperature lift T_3-T_1, but not the mass flow ratio. One common characteristic shown in Figs. 10–12 is that a continued increase of the independent value does not always increase the COP_{gain}. Although Fig. 12 shows this effect for the wave rotor pressure ratio, Fig. 10 reveals a growing gradient of COP_{gain} up to the point where further increase of evaporator temperature actually reduces COP_{gain}. A similar trend can be seen in Fig. 11 where the curves have an asymptotic behavior for increased mass flow ratio.

Figure 13 shows the heat rejecter temperature T_3 versus evaporator temperature for different wave rotor pressure ratios and a constant relative COP_{gain} of 10%. The figure indicates that there are several options for the wave rotor pressure ratio to obtain a certain relative COP_{gain}. However, only the optimum pressure ratio of 2.45 yields the highest temperature lift.

Figure 14 is a performance map of the enhanced cycle. Each

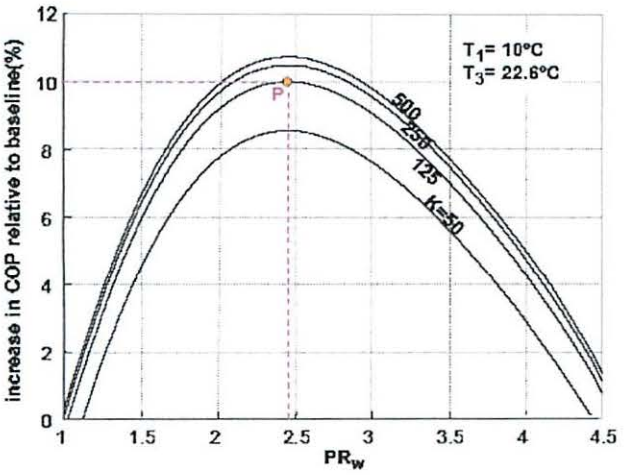

Fig. 12 Relative COP increase versus the wave rotor pressure ratio for different mass flow ratios

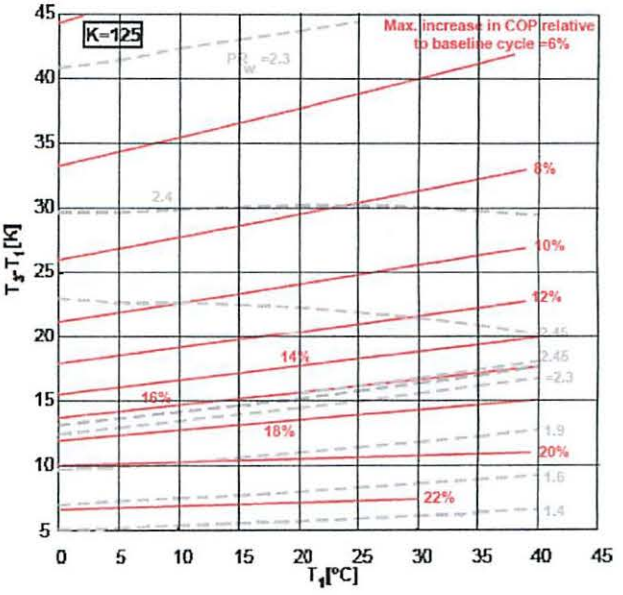

Fig. 14 Performance map: maximum performance increase and optimum wave rotor pressure ratios

Table 3 Calculated baseline cycle state values for the selected optimum point *P*

State	*P* [pa]	*T* [°C]	*h* [kJ/kg]	*s* [kJ/kg K]
1_b	1227	10.0	2519.90	8.90
2_b	4917	179.9	2840.90	9.14
3_b	4917	32.6	136.50	0.47
4_b	1227	10.0	136.50	0.49

point on this plot shows the maximum COP_{gain} that can be obtained by the optimum choice of PR_W for a given evaporator temperature and temperature lift. The constant PR_W lines indicate the optimum PR_W that yields the highest possible COP_{gain} indicated by constant maximum COP_{gain} lines.

In this performance plot of optimized points, an arbitrary optimum point *P* is marked. This point is used to show the connection between all the performance graphs. However, it is the only optimum point in the performance plots of Figs. 10–13. All other points of these plots are not found in Fig. 14 because they show a smaller COP_{gain} than the points in Fig. 14. The calculated state values for the optimum point *P* are tabulated in Tables 3 and 4.

The trend found in Fig. 10 was that for a given T_3 and PR_W, an increase of the evaporator temperature results in a higher COP_{gain}. Such an effect can also be seen in the performance map of the optimized points (Fig. 14) by moving point *P* to the right along constant PR_W line of 2.45. However, for temperature lifts below ~15 K (above maximum COP_{gain} of ~16%) this effect is reversed such that the maximum COP_{gain} decreases with increasing evaporator temperature.

Figure 12 showed that for a given mass flow ratio and a combination of evaporation and heat rejecter temperatures maximum COP_{gain} exists. Since point *P* is at the maximum of the dome, it also appears in Fig. 14.

The following results can be obtained from the performance map of optimized points:

1. The lower the temperature lift, the higher the relative maximum COP_{gain} of the enhanced cycle is.
2. The maximum optimum PR_W for a condensing 3-port wave rotor is about 2.51.
3. Although below a temperature lift of approximately 18 K, the optimum PR_W increases with the temperature lift and decreases slightly for higher temperature lifts. This trend shows a rapidly decreasing gradient with increasing temperature lift.
4. The slope of constant COP_{gain} lines increases as the temperature lift increases, showing that an increase of evaporation temperature is even more beneficial for the enhanced cycle, especially for greater temperature lifts as it is already the case for the R718 baseline cycle.

Summary

In the present study, the advantages of cycles working with water as a refrigerant (R718) and challenges involved with designing them are mentioned. To enhance the turbocompression and improve the efficiency of such cycles, the novel concept of 3-port condensing wave rotors integrated in R718 compression refrigeration cycles is investigated. The condensing wave rotor employs pressurized water to pressurize, desuperheat, and condense the superheated vapor coming from the compressor, all in one dynamic process. The schematic *p-h* and *T-s* diagrams of the external process and the wave and phase-change diagram of the internal process are discussed. Flash evaporation, shock wave compression, desuperheating, and condensation phenomena inside the wave rotor channels are described. A computer code based on a thermodynamic model is developed to evaluate the performance improvement of R718 cycles enhanced cycles. The effect of some key parameters on the performance enhancement is demonstrated as an aid for optimization. Finally, a performance map showing the optimized points of the enhanced cycle is presented. The presented results show an additional improvement of the COP of up to 22% by using the 3-port condensing wave rotor. Besides the performance enhancement, the condensing wave rotor allows lower compressor pressure ratios for the same temperature lift or increases the temperature lift without changing the compressor.

This wave rotor is a simple drum, easy to manufacture, rotating at relatively low speed. Because it performs compression, desuperheating, and condensation in one compact device, it can reduce the size and cost of modern state-of-the-art R718-chillers that now employ high-tech multistage compressors, intercooler, and relative bulky condensers. The details of process inside the wave rotor channels will appreciate more investigations.

Table 4 Calculated enhanced cycle state values for the selected optimum point *P*

State	*P* [pa]	*T* [°C]	*h* [kJ/kg]	*s* [kJ/kg K]
1	1227	10.0	2519.90	8.90
2	2007	61.9	2616.61	8.98
2	4917	154.0	2791.27	9.03
3	4917	32.6	143.77	0.49
5	6307	34.7	145.33	0.50
6	6307	31.7	123.99	0.43
8	1227	10.0	143.77	0.51

References

[1] Griffith, G., 1993, "Alternate Refrigerants for the Refrigeration Industry," *ASHREA-NIST Refrigerants Conference*, pp. 19–28.

[2] Parson, E. A., 2003, *Protecting the Ozone Layer: Science and Strategy*, Oxford University Press, New York.

[3] Kharazi, A. A., Akbari, P., and Müller, N., 2004, "An Application of Wave Rotor Technology for Performance Enhancement of R718 Refrigeration Cycles," *2nd Int. Energy Conversion Engineering Conf.*, AIAA Paper No. 2004–5636.

[4] Kharazi, A. A., Akbari, P., and Müller, N., 2004, "Performance Benefits of R718 Turbo-Compression Cycles Using a 3-Port Condensing Wave Rotors," *2004 Int. Mechanical Engineering Conf.*, ASME Paper No. IMECE2004-609926.

[5] Yuan, Q. S., and Blaise, J. C., 1998, "Water: A Working Fluid for CFC Replacement," Rev. Int. Froid, **11**, pp. 243–248.

[6] Kilicarslan, A., and Müller, N., 2004, "COPs of R718 in Comparison With Other Modern Refrigerants," *First Cappadocia Int. Mechanical Engineering Symp.*, Cappadocia, Turkey.

[7] Rossi, F., and Mastrullo, R., 1991, "Working Fluids Thermodynamic Behavior for Vapor Compression Cycles," Appl. Energy, **38**, pp. 163–180.

[8] Albring, P., 1994, "Water as a Refrigerant in Refrigeration Plants With Mechanical Compression," *New Applications of the Natural Working Fluids in Refrigeration and Air Conditioning, IIR*, Hannover, pp. 735–742.

[9] Albring, P., and Heinrich, G., 1998, "Turbo Chiller With Water as Refrigerant," *Natural Working Fluids'98, IIR*, Oslo, pp. 93–103.

[10] Lachner, B., Nellis, G., and Reindl, D., 2004, "An Investigation Into the Feasibility of the Use of Water as a Refrigerant," *Int. Refrigeration and Air Conditioning Conf.*, Purdue, R160, pp. 1–8.

[11] Müller, N., 2001, "Design of Compressor Impellers for Water as a Refrigerant," ASHRAE Trans., **107**, pp. 214–222.

[12] Wobst, E., Kalitzin, N., and Apley, R., 2005, "Turbo Water Chiller With Water as Refrigerant," *17th Int. Compressor Engineering Conf.*, Purdue, C129.

[13] Weber, H. E., 1995, *Shock Wave Engine Design*, Wiley, New York.

[14] Weber, H. E., 1986, "Shock-Expansion Wave Engines: New Directions for Power Production," ASME Paper No. 86-GT-62.

[15] Akbari, P., Kharazi, A. A., and Müller, N., 2003, "Utilizing Wave Rotor Technology to Enhance the Turbo Compression in Power and Refrigeration Cycles," *2003 International Mechanical Engineering Conf.*, ASME Paper No. IMECE2003-44222.

[16] Taussig, R. T., and Hertzberg, A., 1984, "Wave Rotors for Turbomachinery," *Winter Annual Meeting of ASME*, J. F. Sladky, ed. *Machinery for Direct Fluid-Fluid Energy Exchange*, ASME, New York, Vol. AD-07, pp. 1–7.

[17] Shreeve, R. P., and Mathur, A., 1985, Proc. ONR/NAVAIR Wave Rotor Research and Technology Workshop, Report No. NPS-67-85-008, Naval Postgraduate School, Monterey, CA.

[18] Paxson, D. E., 1995, "Comparison Between Numerically Modeled and Experimentally Measured Wave-Rotor Loss Mechanism," J. Propul. Power, **11**(5), pp. 908–914. See also AIAA Paper No. 93-2522 and NASA TM-106279.

[19] Paxson, D. E., 1996, "Numerical Simulation of Dynamic Wave Rotor Perfor-

mance," J. Propul. Power, **12**(5), pp. 949–957. See also AIAA Paper No. 95-2800 and NASA TM 106997.
[20] Wilson, J., and Paxson, D. E., 1996, "Wave Rotor Optimization for Gas Turbine Topping Cycles," J. Propul. Power, **12**(4), pp. 778–785. See also SAE Paper 951411 and NASA TM 106951.
[21] Welch, G. E., Jones, S. M., and Paxson, D. E., 1997, "Wave Rotor-Enhanced Gas Turbine Engines," ASME J. Eng. Gas Turbines Power, **119**(2), pp. 469–477. See also AIAA Paper 95-2799, and NASA TM 106998.
[22] Welch, G. E., 1997, "Macroscopic Balance Model for Wave Rotors," J. Propul. Power, **13**(4), pp. 508–516. See also AIAA Paper 96-0243, and NASA TM 107114.
[23] Welch, G. E., 1997, "Two-Dimensional Computational Model for Wave Rotor Flow Dynamics," ASME J. Eng. Gas Turbines Power, **119**(4), pp. 978–985. See also ASME Paper No. 96-GT-550 and NASA TM 107192.
[24] Wilson, J., 1998, "An Experimental Determination of Loses in a Three-Port Wave Rotor," ASME J. Eng. Gas Turbines Power, **120**(4), pp. 833–842. See also ASME Paper 96-GT-117, and NASA CR 198456.
[25] Paxson, D. E., and Nalim, M. R., 1999, "Modified Through-Flow Wave-Rotor Cycle With Combustor Bypass Ducts," J. Propul. Power, **15**(3), pp. 462–467. See also AIAA Paper No. 97-3140 and NASA TM 206971.
[26] Welch, G. E., 2000, "Overview of Wave-Rotor Technology for Gas Turbine Engine Topping Cycles," *Novel Aero Propulsion Systems Int. Symp.*, Institution of Mechanical Engineers, pp. 2–17.
[27] Smith, C. F., Snyder, P. H., Emmerson, C. W., and Nalim, M. R., 2002, "Impact of the Constant Volume Combustor on a Supersonic Turbofan Engine," AIAA Paper No. 2002-3916.
[28] Kharazi, A. A., Akbari, P., and Müller, N., 2004, "Preliminary Study of a Novel R718 Turbo-Compression Cycle Using a 3-Port Condensing Wave Rotor," *2004 Int. ASME Turbo Exposition*, ASME Paper No. GT2004-53622.
[29] ILK Dresden, Germany, 2004, "R718-Turbo-Chiller System Dimensions," Company Brochure, R718-Turbo-A626 (ATV110/1-25-52 and ATV110/3-21-52).
[30] Saury, D., Harmand, S., and Siroux, M., 2001, "Experimental Study of Flash Evaporation of Water Film," Int. J. Heat Mass Transfer, **45**, pp. 3447–3457.
[31] Miyatake, O., Murakami, K., and Kawata, Y., 1973, "Fundamental Experiments With Flash Evaporation," Heat Transfer-Jpn. Res., **2**, pp. 89–100.
[32] Anderson, J. D., 2003, *Modern Compressible Flow*, Third Edition, McGraw-Hill, New York.

Amir Kharazi *is an Aerodynamicist and CFD Engineer at Jacobs Engineering Group, working on the design and operation of wind tunnels and automotive test facilities. His research interests include R718 refrigeration cycles, turbomachinery, and wind tunnels. He is the lead author for several journal and conference papers and received the NSF/JSPS research fellowship in 2005. Kharazi received his Ph.D. in Mechanical Engineering from Michigan State University in 2006.*

Pezhman Akbari *is currently a Postdoctoral Research Fellow at Indiana University Purdue University Indianapolis (IUPUI), working on design and modeling of rotary pressure gain turbine engines. He has a B.S. and M.S. degrees in Aerospace Engineering, and a Ph.D. in Mechanical Engineering from Michigan State University. He is the author of more than 20 papers related to unsteady wave devices that have been presented at various international conferences and/or published in journals, including those of ASME, AIAA, and IGTC. In 2003, he received the AIAA Foundation Graduate Award for studies in the potential of wave devices in gas turbines.*

Norbert Müller *is an Assistant Professor of Mechanical Engineering. He received his Ph.D. from Technische Universität Dresden, Germany, in 1999. His research focuses on turbomachinery, wave rotors, centrifugal compressors, refrigeration systems, microfabricated energy systems, and heat exchangers. From 1993 to 1999, he worked for the industrial research center Institut für Luft- und Kältetechnik (ILK) Dresden. He has also worked in Aerospace at MTU Aero Engines in Munich, and at Bath University in Great Britain. Just prior to joining Michigan State University, he was an Adjunct Assistant Professor and a Research Scientist at Columbia University.*

Sandia National Laboratories

NATIONAL SOLAR THERMAL TEST FACILITY

Related Links

Home

National Solar Thermal Test Facility

Links

Advantages of Using Molten Salt

A variety of fluids was tested to transport the sun's heat, including water, air, oil, and sodium, before molten salt was selected as best. Molten salt is used in solar power tower systems because it is liquid at atmosphere pressure, it provides an efficient, low-cost medium in which to store thermal energy, its operating temperatures are compatible with todays high-pressure and high-temperature steam turbines, and it is non-flammable and nontoxic. In addition, molten salt is used in the chemical and metals industries as a heat-transport fluid, so experience with molten-salt systems exists for non-solar applications.

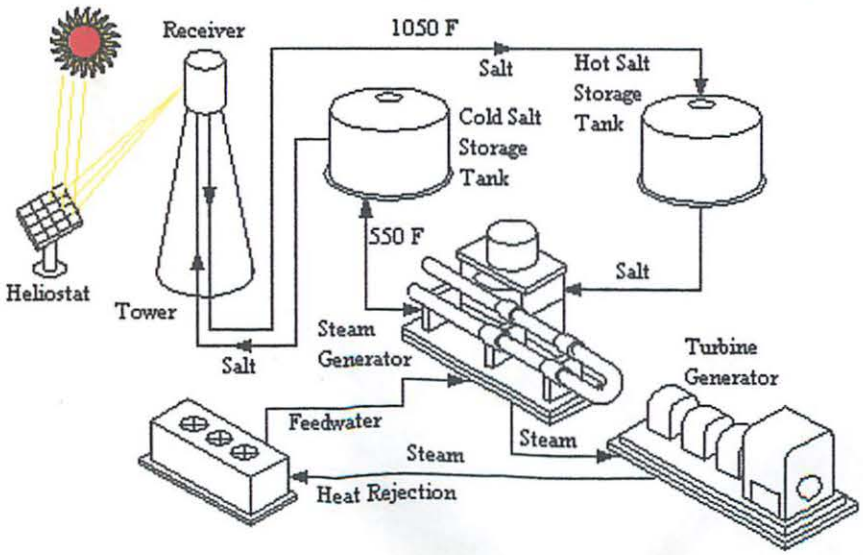

Contact:
Tom Mancini
Sandia National Laboratories,
Mail Stop 1127
Albuquerque, NM 87185
Phone: 505-844-8643
FAX: 505-845-3366
E-Mail: trmanci@sandia.gov

The molten salt is a mixture of 60 percent sodium nitrate and 40 percent potassium-nitrate, commonly called saltpeter. The salt melts at 430 F and is kept liquid at 550 F in an insulated cold storage tank. The salt is them pumped to the top of the tower, where concentrated sunlight heats it in a receiver to 1050 F. The receiver is a series of thin-walled stainless steel tubes. The heated salt then flow back down to a second insulated hot storage tank. The size of this tank depends on the requirements of the utility; tanks can be designed with enough capacity to power a turbine from two to twelve hours. When electricity is needed from the plant, the hot salt is pumped to a conventional steam-generating system to produce superheated steam for a turbine/generator.

The uniqueness of this solar system is in de-coupling the collection of solar energy from producing power, electricity can be generated in periods of inclement weather or even at night using the stored thermal energy in the hot salt tank. The tanks are well insulated and can store energy for up to a week. As an example of their size, tanks that provide enough thermal storage to power a 100-megawatt turbine for four hours would be about 30 feet tall and 80 feet in diameter. Studies show that the two-tank storage system could have an annual efficiency of about 99 percent.

Top of page

Lisa Sena-Henderson

Last Modified: 01/10/06

Sandia National Laboratories

NATIONAL SOLAR THERMAL TEST FACILITY

Advantages of Using Molten Salt

A variety of fluids was tested to transport the sun's heat, including water, air, oil, sodium, before molten salt was selected as best. Molten salt is used in solar power to systems because it is liquid at atmosphere pressure, it provides an efficient, low-c medium in which to store thermal energy, its operating temperatures are compatible v todays high-pressure and high-temperature steam turbines, and it is non-flammable nontoxic. In addition, molten salt is used in the chemical and metals industries as a he transport fluid, so experience with molten-salt systems exists for non-solar applicatic

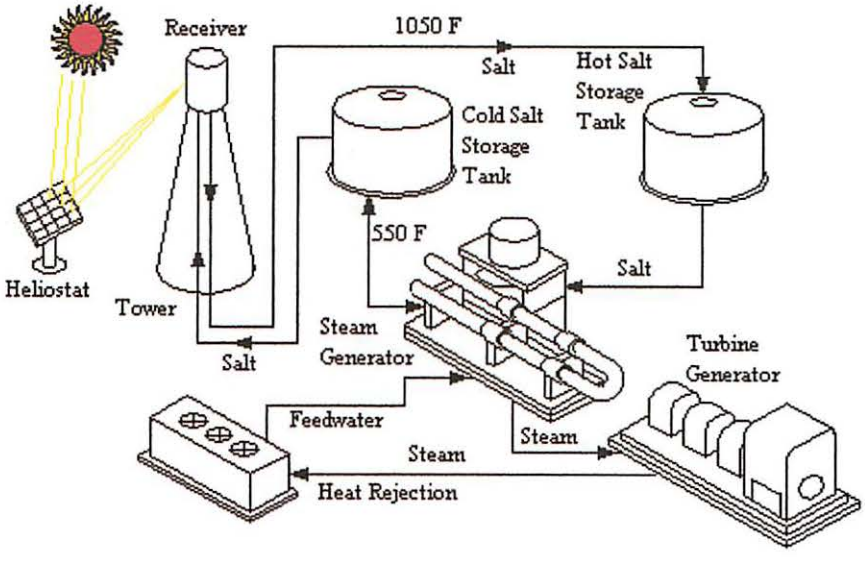

The molten salt is a mixture of 60 percent sodium nitrate and 40 percent potassiu nitrate, commonly called saltpeter. The salt melts at 430 F and is kept liquid at 550 I an insulated cold storage tank. The salt is them pumped to the top of the tower, wh concentrated sunlight heats it in a receiver to 1050 F. The receiver is a series of th walled stainless steel tubes. The heated salt then flow back down to a second insula hot storage tank. The size of this tank depends on the requirements of the utility; ta can be designed with enough capacity to power a turbine from two to twelve hours. Wl electricity is needed from the plant, the hot salt is pumped to a conventional stea generating system to produce superheated steam for a turbine/generator.

The uniqueness of this solar system is in de-coupling the collection of solar energy fr producing power, electricity can be generated in periods of inclement weather or ever

night using the stored thermal energy in the hot salt tank. The tanks are well insula and can store energy for up to a week. As an example of their size, tanks that prov enough thermal storage to power a 100-megawatt turbine for four hours would be ab 30 feet tall and 80 feet in diameter. Studies show that the two-tank storage system cc have an annual efficiency of about 99 percent.

Top of page

Lisa Sena-Henderson

Last Modified: 01/10/06

RESEARCH IN MICROFLUIDIC TRANSPORT AT SANDIA NATIONAL LABORATORIES

Hydrogen Production

Thermal redox systems for solar hydrogen generation

We are developing a rational design approach to thermal redox systems for the production of hydrogen. Currently, we are using thermodynamic analysis of mixed-metal ferrite systems (e.g. AFe_2O_4, A = Mg, Co, Ni, or Zn) to determine optimal conditions for material synthesis, thermal reduction, and hydrogen production. Redox cycles using iron-containing ferrites are being proposed for two-step water-splitting cycles for the production of hydrogen from solar energy. These cycles consist of a thermal reduction step (TR; reaction (1)) in which solar energy is used to reduce the Fe(III) to the Fe(II) state with release of O_2, followed by a water oxidation step (WO; reaction (2)) in which the reduced oxide reacts with steam to form hydrogen and regenerate the ferrite:

$$A_xFe_{3-x}O_4 \xrightarrow{\Delta} xAO + (3-x)FeO + 0.5\ O_2 \qquad (1)$$

$$xAO + (3-x)FeO + H_2O \longrightarrow A_xFe_{3-x}O_4 + H_2 \qquad (2)$$

Our calculations are proving to be a valuable tool for selecting materials. For example, the results suggest that zirconia ceramic supports play both a chemical as well as physical role in the redox process and that $NiFe_2O_4$ displays the best overall combination of properties for solar redox cycles (see **Fig. 1**).

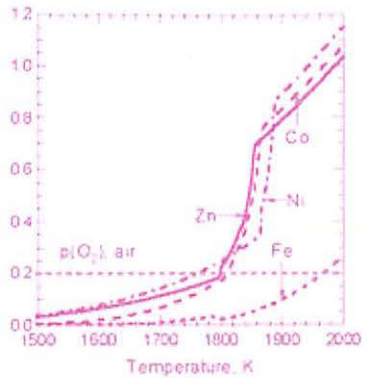

Figure 1. Comparison of oxygen partial pressures in equilibrium with various metal-substituted ferrites (MFe_2O_4). The dashed blue line indicates $p(O_2)$ for air, showing the temperature at which a given ferrite can be reduced to suboxides (FeO + MO) in air.

Publications

R.B. Diver, J.E. Miller, M.D. Allendorf, N.P. Siegel, R.E. Hogan "Solar Thermochemical Water-Splitting Ferrite-Cycle Heat Engines," *J. Solar En. Eng.* in press, August 2008.

M. D. Allendorf, R. B. Diver, N. P. Siegel, J. E. Miller "Two-Step Water Splitting Using Mixed-Metal Ferrites: Thermodynamic Analysis and Characterization of Synthesized Materials," in press, *Energy and Fuels* Sept. 2008.

J. E. Miller, M. D. Allendorf, R. B. Diver, L. R. Evans, N. P. Siegel and J. N. Stuecker "Metal oxide composites and structures for ultra-high temperature solar thermochemical cycles," *J. Mater. Sci.*, Volume: **43** Issue: **14** Pages: **4714-4728** 2008.

M. D. Allendorf, J. E. Miller, N. P. Siegle, R. B. Diver Jr. "Thermodynamic Analysis Of Mixed-Metal Ferrites For Hydrogen Production By Two-Step Water Splitting," *Proc. ISEC 2006*, ISEC2006-99114.

J. E. Miller, L. R. Evans, J. N. Stuecker, M. D. Allendorf, N. P. Siegel, and R. B. Diver "Materials Development for the CR5 Solar Thermochemical Heat Engine," *Proc. ISEC 2006*, ISEC2006-99152.

R. B. Diver Jr., J. A. Miller, M. D. Allendorf, N. P. Siegel, R. E. Hogan "Solar Thermochemical Water-Splitting Ferrite-Cycle Heat Engines," *Proc. ISEC 2006*, ISEC2006-99147.

Photovoltaics

Concentrating Solar Power

Research & Development
- Linear Concentrators
- Dish/Engines
- Power Towers
- Thermal Storage
- Components & Systems

Systems Integration

Market Transformation

Thermal Storage Research and Development

As part of its research program in concentrating solar power (CSP), the U.S Department of Energy (DOE) sponsors research and development (R&D) for thermal storage. The key goals for thermal storage R&D are to

- Support industry in developing and deploying advanced heat-transfer fluids and thermal storage systems
- Develop and characterize advanced heat-transfer fluids and thermal-storage materials and systems to reduce storage costs
- Update and integrate thermal storage cost and performance models into CSP system models.

This page summarizes key thermal storage R&D activities by the National Renewable Energy Laboratory (NREL) and Sandia National Laboratories to attain the above goals in three areas:

- Storage systems
- Advanced heat-transfer fluids
- Industry support.

Storage Systems R&D

Storage systems R&D focuses on systems analysis issues that relate to evaluating and improving the performance and cost of thermal storage systems for parabolic trough power plants. Representative projects in this area include the following:

Thermal Energy Storage Cost Analysis

We are developing a cost model for storage that determines the capital costs of thermal energy storage based on the quantities of commodity materials used to construct and operate the system. Capital costs for the systems can then be updated simply by updating the costs of the required commodity materials. The method considers the practical limits of tank size, including stress constraints and commercial availability.

Thermal Energy Storage Modeling

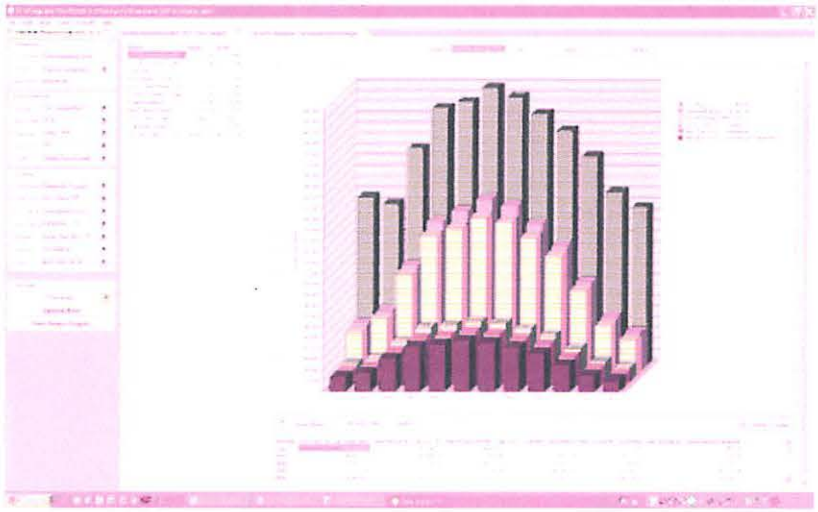

Specially developed computer software helps to model and analyze the cost for CSP, including the impact of thermal energy storage.

We model heat-transfer and fluid dynamics within thermal storage systems to better evaluate operation and overall system performance. Comparative modeling of heat transfer and fluid dynamics of the two-tank and thermocline storage systems helps to determine relative performance benefits and to optimize storage configurations and operational strategies. The analysis considers total storage requirements, charging and discharging power requirements, storage-vessel size limitations, vessel orientation, and aspect ratio. Our goal is to determine the optimal storage configurations for likely solar field sizes that minimize the levelized cost of electricity.

Advanced Heat-Transfer Fluids R&D

Advanced heat-transfer fluids are essential for improving the operation of CSP systems. Historically, trough systems have used synthetic heat-transfer oils, power towers have demonstrated direct steam generation and molten-salt working fluids, and dish/engine systems have used hydrogen and helium as working fluids. We are developing heat-transfer and storage fluids that provide improved efficiency and lower cost for CSP systems. Representative projects in this area include the following:

Nitrate Salt Formulations

Sandia has developed and characterized a new low-freezing (100°C) nitrate salt formulation. Researchers are now characterizing the properties and performance of their new nitrate salt formulation for use in parabolic trough power plants.

Nanofluids

Solutia Inc.'s Therminol VP-1 is the current heat-transfer fluid of choice in parabolic trough solar fields. It is thermally stable to about 400°C

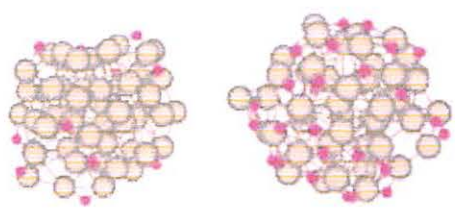

Aluminum nanoclusters can be tailored

and has a low freezing point of 12° C. NREL is studying a new class of nanofluids that possess enhanced thermophysical properties including thermal conductivity, heat capacity, freezing point, boiling point, and high-temperature thermal stability. One goal is to develop heat-transfer fluids with higher operating temperatures, which allow a plant to operate with greater efficiency. A second goal is to develop storage fluids with higher heat capacities, which allow the use of much less storage fluid for the same amount of storage capacity.

for unique thermochemical properties.

Non-Nitrate Molten-Salt Fluids
We are pursuing non-nitrate salts and other inorganic substances as heat-transfer and storage fluids. We are identifying candidates that possess the thermophysical and fluid properties of the current nitrate salts, but without the potential corrosive properties of some nitrate salts.

Materials Laboratory for Thermal Storage
We are establishing a materials laboratory to develop and characterize advanced heat-transfer fluids, advanced storage fluids, and advanced phase-change materials for thermal storage applications. These materials will lead to increased thermal storage capacity, thermodynamic efficiency, and dispatchability, as well as lower levelized energy costs for CSP power plants.

Laboratory capabilities will support experiments and validate molecular dynamic modeling studies of nanophase materials and will allow the study of novel phase-change materials. Such materials are essential for implementing thermal storage that is compatible with direct steam generation—which is being considered as the next-generation heat-transfer fluid for parabolic trough power plants.

Industry Support

NREL and Sandia provide technical testing and evaluation support to its industry partners. DOE also coordinates industry support for CSP thermal energy storage as it collaborates with national laboratories in Europe—CIEMAT in Spain and DLR in Germany.

Some of DOE's technical activities support the awardees of financial opportunities for concentrating solar power. The complete list of DOE-funded CSP projects is available on the Concentrating Solar Power Industry Projects page that specifically includes the thermal storage projects.

Printable Version

Largest Solar Thermal Storage Plant to Start Up

By **Peter Fairley**

PHOTO: SOLAR MILLENNIUM

1 October 2008—A few weeks from now, the Andasol 1 solar thermal power plant in Andalucia, Spain, will begin charging the largest installation built expressly for storing renewable energy (other than the tried-and-true hydroelectric dam, of course). Heat from the solar thermal power station's 510 000-square-meter field of solar collectors will be stored in 28 500 tons of molten salt—enough to run the plant's 50-megawatt steam turbine for up to 7.5 hours *after dark*.

It's pretty strange for solar power to generate electricity in the dark. Stranger still for a renewable-energy project is the fact that Andasol 1's developers—German renewable-energy firm Solar Millennium and Madrid-based engineering and construction firm ACS/Cobra—believe the energy storage that makes the plant's output more predictable will also make it more affordable. The developers say Andasol 1's electricity will cost 11 percent less to produce than a similar plant without energy storage—dropping from 303 euros per megawatt-hour to 271 euros per MWh.

The lower cost of production is actually a by-product of Andasol 1's energy-storage system, according to Paul Nava, a managing director of Flagsol GmbH, the Cologne, Germany–based engineering subsidiary of Solar Millennium that designed the plant. Nava says storage is a means of maximizing the net energy production from each plant and thus maximizes the revenues paid under Spain's generous incentive program for renewable-energy generation. A feed-in tariff for solar thermal power pays 2.5 to 3 times the average power price for every MWh of energy generated for 25 years (though new rules will reduce the rate for future projects) but limits the capacity of qualifying facilities to 50 MW. Storage enables Andasol 1 to run its 50-MW turbine for more hours.

Nava estimates that Andasol 1 will generate 178 000 MWh of renewable electricity per year, whereas the same field of solar collectors and turbine would turn out just 117 000 MWh sans storage—a difference worth more than 24 million euros per year (US $36 million) at today's power prices.

At Andasol 1, generating this clean energy surplus starts with 24 kilometers of trough-shaped mirrors concentrating sunlight on solar collector tubes and heating the synthetic oil flowing within as high as 400 degrees Celsius (the safety and durability limit for the oil). To put power on the grid, hot oil is circulated to the plant's "power block," where the heat is converted to steam and drives the turbine. However, when the sun is strongest, Andasol 1's oversized collector field should gather almost twice as much heat as the turbine can handle. This extra heat will be dumped into the storage system: a heat exchanger connecting two insulated storage tanks, each 14 meters high and 36 meters in diameter, holding molten potassium and sodium nitrate salt.

The tanks are kept at different temperatures. Molten salt pumped from the "cold" tank (maintained at a not-so-chilly 260 °C to keep the salt molten) into the heat exchanger picks up heat from the oil and then flows into the hot tank (which will reach 400 °C when fully charged). To discharge the stored energy, the process is reversed, with molten salt pumped from the hot tank to the cold tank to reheat the oil.

One problem with running a molten-salt storage system is that the salt could freeze during cold snaps, necessitating an injection of heat that reduces the plant's power output. But Nava says Andasol 1 has some improvements over earlier experimental designs to minimize the need to warm the salt. Andasol 1's valves are fewer in number, and both the valves and the heat exchanger are designed to drain when not in use, eliminating the need to keep them hot. The pumps, which cannot be drained regularly, sit submerged within the tanks instead of outside the tanks, where they would have to be heated separately. Nava estimates that, overall, annual energy losses from the storage system will be just 5 percent.

More such plants are on the way in Spain. Solar Millennium and its Spanish partner expect to start up a twin plant, Andasol 2, next spring and plan to begin building a third 50-MW plant early next year.

Spain's Abengoa Solar and Sener, meanwhile, are each testing solar thermal plants with integrated molten-salt storage. Both use a "power tower" configuration in which arrays of mirrors direct sunlight onto a central solar receiver where the light directly heats a molten salt. This configuration matches that of Solar Two, a 10-MW solar thermal demonstration plant at Sandia National Laboratories, in New Mexico, built in the 1990s. The power-tower design makes energy storage cheaper and more compact because the salts can be safely heated well beyond the limit of the synthetic oils.

"Using the molten salt as both the working and storage fluid gave us high heat capacity," says Sandia concentrating solar-power program manager Thomas Mancini. "Instead of 260 °C to 390 °C, you're going from 260 °C to 560 °C. It's a bigger temperature difference, so you need less salt to store the same amount of energy."

At present, most of the anticipated U.S. solar thermal projects, which are driven by state-level renewable-energy mandates rather than a rich feed-in tariff, are focused on minimizing upfront costs, and few projects plan to integrate energy storage. But Mancini and Nava say that may change as utilities adopt time-of-day electricity pricing.

Nava says a pricing scheme already introduced by Southern California Edison should encourage what he calls a "solar booster" thermal power plant. The California utility pays 3.28 times its base rate for electricity delivered between noon and 6 p.m. on summer weekdays. A solar booster would use an undersized collector field and storage to focus generation on that sweet spot. "In the morning, you use the solar field only to charge the storage, and then from noon on, when you have that factor of three for the electricity rate, you discharge the storage and use the field in parallel to drive the steam turbine," says Nava.

About the Author

Contributing Editor Peter Fairley has reported for *IEEE Spectrum* from Bolivia, Beijing, and Paris. In May 2008 he wrote for us about China's rapid gains in wind power.